PHOTOCHEMICAL ESCAPE OF THE MARTIAN ATMOSPHERE, TODAY AND THROUGH TIME.

R. J. Lillis[1], J. Deighan[2], J. L. Fox[3], S.W. Bougher[4], Y. Lee[4], M. Combi[4], F. Leblanc[5], T. E. Cravens[6], A. Rahmati[6], B. M. Jakosky[2] [1]UC Berkeley Space Sciences Laboratory (rlillis@ssl.berkeley.edu), [2]Laboratory for Atmospheric and Space Physics, University of Colorado Boulder, [3]Department of Physics, Wright State University, [4]Department of Atmospheric, Oceanic and Space Sciences, University of Michigan, [5]Laboratoire de Météorologie Dynamique, Jussieu, Paris [6]Department of Physics and Astronomy, University of Kansas.

Introduction: Photochemical escape in planetary atmospheres is a process by which a) an exothermic chemical reaction produces an upward-traveling neutral particle whose velocity exceeds the planetary escape velocity and b) the particle is not prevented from escaping through any subsequent collisions with thermal neutrals. At Mars, photochemical escape is thought to be the dominant loss process for neutrals heavier than hydrogen today [*Lammer et al.*, 2008], likely several times larger than heavy ion escape, and thus one of the major pathways for atmospheric escape over the history of Mars. By approximately 2 orders of magnitude the dominant escaping atom is O (cf. table 3 of *Brain et al.* [2015]), mostly the result of DR of O_2^+, the process upon which we will focus in this study.

The critical altitude region for photochemical escape is within a few scale heights of the exobase (i.e. 170-250 km), i.e. the region sufficiently low in altitude that substantial amounts of O_2^+ are created, but where the mean free path is sufficiently large that energized hot O atoms can escape the atmosphere in substantial numbers without first losing too much energy through collisions.

Several numerical models of photochemical escape of O from Mars have been developed in recent years using input from the two vertical profiles recorded by the Viking Landers [*Hanson et al.*, 1976; *Nier et al.*, 1976] and global circulation models [*Bougher et al.*, 1999; 2000; *Gonzalez-Galindo et al.*, 2013]. Photochemical escape rates range from 1.0 to 6.0 x 10^{25} s^{-1} for equinox solar minimum conditions and from 4.0 to 22.0 x 10^{25} s^{-1} for equinox solar maximum conditions, with an average of 2.75 for the ratio between the former and latter conditions.

Data used in this study. Although photochemical escape of O cannot be directly measured by MAVEN, all of the important quantities upon which it depends are measured in situ in the Mars upper atmosphere, typically on at least every other orbit. We use in situ data from three instruments collected below 400 km during 1982 orbits orbits spanning February 11 2015 to June 28 2016. We obtain temperatures and densities of ambient electrons measured by the Langmuir Probe and Waves (LPW) experiment [*Andersson et al.*, 2015]. We also use temperatures of thermal O_2^+ ions measured by the SupraThermal And Thermal Ion Composition (STATIC) experiment [*McFadden et al.*, 2015]. Finally, we use densities of thermal O_2+ ions and the thermal neutral species CO_2, CO, N_2 and O measured by the Neutral Gas and Ion Mass Spectrometer (NGIMS) [*Mahaffy et al.*, 2014]

We note that NGIMS cannot measure both ions and reactive neutral species (i.e. CO and O) on the same periapsis pass. For this reason, we use different subsets of the 1982 orbits to calculate dissociative recombination rates and escape probabilities, according to the availability of the relevant data in each set of orbits, as discussed in the next section.

Method for calculating escape fluxes.

In order to determine photochemical escape fluxes of hot oxygen from in situ measurements, we separately calculate two different quantities as a function of altitude z: 1) the production rate of hot oxygen atoms from O2+ DR and 2) the probability that, once produced, a hot O atom will escape the atmosphere. DR occurs via 4 main channels with the resulting O atoms each leaving with half of the exothermic energy in the center of mass frame of the electron-ion collision. The four channels are given:

Initial state	Final state	Likelihood
$O_2^+ + e \rightarrow$	$O(^3P) + O(^3P) + 6.99$ eV	26.5%
	$O(^1D) + O(^3P) + 5.02$ eV	47.3%
	$O(^1D) + O(^1D) + 3.06$ eV	20.4%
	$O(^1D) + O(^1S) + 0.83$ eV	5.8%

Figure 1: channels and ratios for DR of O2+

The upper two of these reactions result in individual O energies in excess of the escape energy (at 200 km altitude) of 1.98 eV. For each set of neutral density and electron and ion temperature profiles, we run a three-dimensional Monte Carlo hot atom transport model to calculate escape probabilities as a function of altitude. We assume the atmosphere is spherically symmetric with the same altitude profile

everywhere. Hot O atoms start at a set altitude and are given random directions and an initial energy drawn at random from the initial energy distribution for that altitude (mentioned in the previous paragraph). They are propagated through collisions with thermal neutrals until 2500 escape, from which escape property is calculated. We run this model at each altitude starting from 400 km we work down in altitude until the escape probability falls below 5e-5.

Once we have calculated altitude profiles of the hot O production rate and the hot O escape probability, we simply multiply these two quantities together at each altitude step to get the production rate of escaping hot O. We then integrate with respect to altitude to get the hot O escape flux for that particular periapsis pass. Figure 1 is a flowchart of this calculation, relating the quantities measured by MAVEN, formulae derived from experiment, models and calculated values.

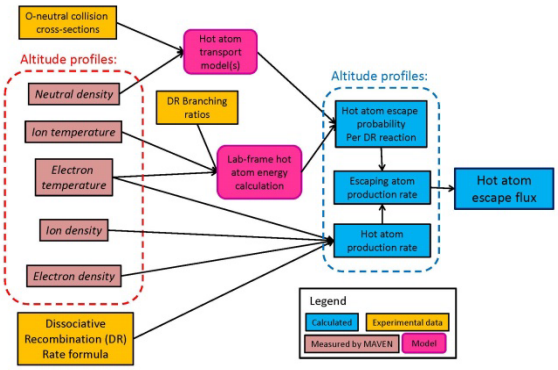

Figure 2: Flowchart explaining calculation of hot oxygen escape from measured altitude profiles of neutral densities and ion and electron densities and temperatures.

The profiles of all necessary quantities shown in the left magenta boxes in Figure 2 are not measured in the same orbit. Therefore, for each of the 951 orbits where we are able to determine the hot oxygen production rate profile (see the lower blue box in Figure 2), we multiply by an escape probability profile (upper blue box in Figure 2) that is the mean of the escape probability profiles determined from the previous and subsequent orbits.

Dependence on EUV flux: Escape fluxes show a positive trend with respect to solar EUV flux measured at Mars. Figure 3a shows all 951of the derived values of O escape flux taken with solar zenith angles less than 90° (no significant dependence of derived escape flux on solar zenith angle was observed within this range), i.e. dayside, as a function of the EUV irradiance at 30.4 nm estimated by the FISM-M model [Thiemann et al., 2016], along with binned averages and standard deviations. Power law fits to this data were then tried for a wide range of power law indices. Reduced chi-square values were calculated assuming an error of 0.3 x 10^7 $cm^{-2}s^{-1}$ for every point, which is approximately the spread in values collected within the same day. The best fit index is 2.19, but with quite a large spread (1.2 to 3.0) within 1-sigma. The dip that we see for intermediate values of 30.4 nm flux is likely due to seasonal effects, i.e. the lower atmosphere respond more slowly solar IR flux than the upper atmosphere does to solar EUV flux. Only by collecting data over multiple Mars years will we be able to disentangle seasonal from solar cycle effects.

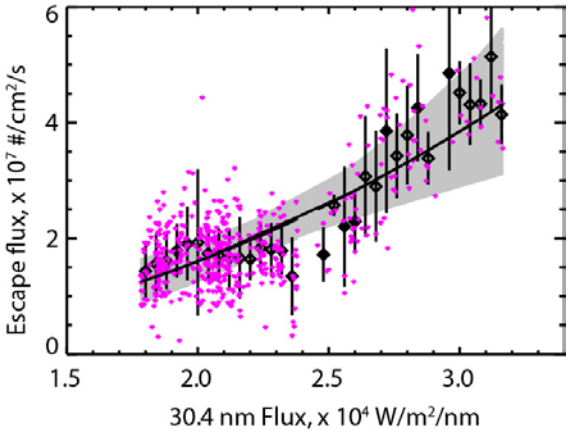

Figure 3: Dependence of dayside O escape fluxes on 30.4 nm EUV irradiance. We show all 951 individual derived escape flux values (small pink dots) and binned values (black diamonds) with standard deviations in each bin. All fits to this data that fall within the 1-sigma error ellipsoid are shown as gray lines, with the best fit (power law index of 1.76) shown in black.

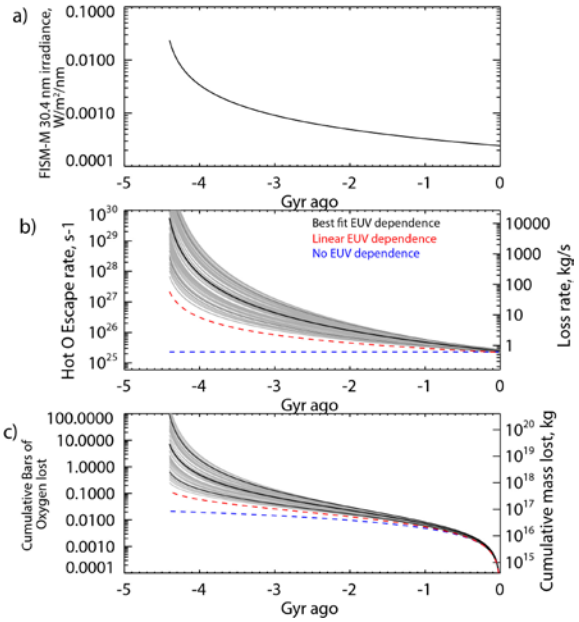

Figure 4: Extrapolation of photochemical O escape rates over Martian history. Panel a) shows the assumed history of 30.4 nm EUV irradiance, taken from *Ribas et al.* [2005]. Panels b) and c) shows the resulting escape rates and cumulative oxygen lost respectively, assuming the best power law fit (1.78) to EUV dependence (thick black), the range of 1-sigma power law fits, the 10th and 90th percentiles of those distributions (thin black), a linear dependence (red dashed) [*Cravens et al.*, 2016] and no EUV dependence, i.e. a simple extrapolation back in time of the present-day escape rate (blue dashed).

Modern-day EUV flux: One of the prime goals of the MAVEN mission is to constrain the total loss of atmosphere over Martian history. In order to build a baseline from which we may extrapolate photochemical O escape rates backward in time, we must estimate the average escape rate over the modern epoch, i.e. over the range of solar EUV irradiance conditions that exist in the modern era. We use the weekly irradiance at 30.4 nm calculated at Mars by FISM-M since 1947 on the basis of direct measurements back to 2002, satellite measurements of solar Lyman alpha irradiance back to 1978 and ground-based measurements of F10.7 solar radio flux prior to 1978 [*Thiemann et al.*, 2016]. 80% of values lie within the range of 1.2 to 4.5 x 10^{25} s^{-1}.

Historical Loss of atomic oxygen over time: We now have in hand a modern-day estimate for photochemical escape rates and a range of dependences on EUV flux. This allows us to make estimates of escape rates at earlier times in solar system history. We utilize a functional form for the evolution of EUV irradiance with stellar age derived by Ribas et al. [2005] from observations of six sun-like stars with a range of ages from 0.1 to 6.7 Gyr. They determined that irradiance in the wavelength range 10-36 nm (which encompasses the solar 30.4 nm He II line we are using) decreases as $t^{-1.2}$, where t is the stellar age in billions of years. We set the irradiance at t = 4.5 Gyr (i.e. the present-day) to be the mean of the 30.4 nm irradiance from the 70-year reconstructed record FISM-M shown in Figure 6a: 0.000244 $W/m^2/nm$. The resulting estimate of 30.4 nm irradiance over solar system history is shown in Figure 4a. We then use the best-fit and 1-sigma range of power law indices to extrapolate O escape rates and cumulative loss back to 4.4 Gyr ago, shown in Figure 4b and c respectively. For comparison, we also show the simplistic case of simply extrapolating current escape rates back to the early solar system (blue dashed lines) and a linear EUV dependence from the theoretical result of [*Cravens et al.*, 2016](red dashed lines).

We notice a few features in these extrapolations. The first is that the simply extrapolating current escape rates backwards in time (thereby assuming no EUV dependence) leads to unrealistically low escape rates and cumulative loss amounts. Secondly, the range of escape rates and cumulative losses is relatively narrow back to ~3 Gyr, but then rapidly increases as EUV irradiance increases, due to the broad range of power law fits that are consistent with the MAVEN data. For example, 12 times higher EUV at 4 Gyr ago leads to ~19 times higher escape if the power law index 1.2, but 235 times higher if the index is 2.2. Therefore, better constraining the EUV dependence of photochemical escape rates is a primary concern as more data is collected during MAVEN's extended mission. In particular, disentangling seasonal from solar cycle effects may require more than one Mars year of observations.

References:

Andersson, L., R. E. Ergun, G. T. Delory, A. Eriksson, J. Westfall, H. Reed, J. McCauly, D. Summers, and D. Meyers (2015), The Langmuir Probe and Waves (LPW) Instrument for MAVEN, *Space Science Reviews*, *195*(1), 173-198, doi:10.1007/s11214-015-0194-3.

Bougher, S. W., S. Engel, R. G. Roble, and B. Foster (1999), Comparative terrestrial planet thermospheres 2. Solar cycle variation of global structure and winds at equinox, *Journal of Geophysical Research-Planets*, *104*(E7), 16591-16611, doi:Doi 10.1029/1998je001019.

Bougher, S. W., S. Engel, R. G. Roble, and B. Foster (2000), Comparative terrestrial planet thermospheres 3. Solar cycle variation of global structure and winds at solstices, *Journal of Geophysical Research-Planets*, *105*(E7), 17669-17692, doi:Doi 10.1029/1999je001232.

Brain, D. A., S. Barabash, S. W. Bougher, F. Duru, B. M. Jakosky, and R. Modolo (2015), Solar Wind Interaction and Atmospheric Escape, in *Mars book II*, edited.

Cravens, T., et al. (2016), Oxygen escape from Mars, *Journal of Geophysical Research, in press*.

Gonzalez-Galindo, F., J. Y. Chaufray, M. A. Lopez-Valverde, G. Gilli, F. Forget, F. Leblanc, R. Modolo, S. Hess, and M. Yagi (2013), Three-dimensional Martian ionosphere model: I. The photochemical ionosphere below 180 km, *Journal of Geophysical Research-Planets*, *118*(10), 2105-2123, doi:Doi 10.1002/Jgre.20150.

Hanson, W. B., S. Sanatani, and D. Zuccaro (1976), Retarding Potential Analyzer Measurements from Viking Landers, *Transactions-American Geophysical Union*, *57*(12), 966-966.

Lammer, H., J. F. Kasting, E. Chassefiere, R. E. Johnson, Y. N. Kulikov, and F. Tian (2008), Atmospheric Escape and Evolution of Terrestrial Planets and Satellites, *Space Science Reviews*, *139*(1), 399-436, doi:10.1007/978-0-387-87825-6_11.

Mahaffy, P. R., et al. (2014), The Neutral Gas and Ion Mass Spectrometer on the Mars Atmosphere and Volatile Evolution Mission, *Space Science Reviews*, *195*(1), 49-73, doi:10.1007/s11214-014-0091-1.

McFadden, J. P., et al. (2015), MAVEN SupraThermal and Thermal Ion Compostion (STATIC) Instrument, *Space Science Reviews*, *195*(1), 199-256, doi:10.1007/s11214-015-0175-6.

Nier, A. O., W. B. Hanson, A. Seiff, M. B. Mcelroy, N. W. Spencer, R. J. Duckett, T. C. D. Knight,

and W. S. Cook (1976), Composition and Structure of Martian Atmosphere - Preliminary-Results from Viking-1, *Science, 193*(4255), 786-788, doi:DOI 10.1126/science.193.4255.786.

Ribas, I., E. F. Guinan, M. Güdel, and M. Audard (2005), Evolution of the Solar Activity over Time and Effects on Planetary Atmospheres. I. High-Energy Irradiances (1-1700 Å), *The Astrophysical Journal*, *622*(1), 680.

Thiemann, E., P. Chamberlin, F. Eparvier, T. Woods, S. Bougher, and B. Jakosky (2016), The MAVEN/EUVM Level 3 Spectral Irradiance Model: Algorithms and Results, *Journal of Geophysical Research*.